Mon. Not. R. Astron. Soc. **313**, 229–236 (2000)

Peculiar velocities of galaxy clusters

J. M. Colberg,[1] S. D. M. White,[1★] T. J. MacFarland,[2†] A. Jenkins,[3] F. R. Pearce,[3] C. S. Frenk,[3] P. A. Thomas[4] and H. M. P. Couchman[5]

[1]*Max-Planck-Institut für Astrophysik, Karl-Schwarzschild-Str. 1, D-85740 Garching, Germany*
[2]*Rechenzentrum Garching, Boltzmannstr. 2, D-85740 Garching, Germany*
[3]*Physics Department, University of Durham, Durham DH1 3LE*
[4]*CEPS, University of Sussex, Brighton BN1 9QH*
[5]*Department of Physics and Astronomy, McMaster University, Hamilton, Ontario L8S 4M1, Canada*

Accepted 1999 October 11. Received 1999 June 28; in original form 1998 May 13

ABSTRACT

We investigate the peculiar velocities predicted for galaxy clusters by theories in the cold dark matter family. A widely used hypothesis identifies rich clusters with high peaks of a suitably smoothed version of the linear density fluctuation field. Their peculiar velocities are then obtained by extrapolating the similarly smoothed linear peculiar velocities at the positions of these peaks. We test these ideas using large high-resolution *N*-body simulations carried out within the Virgo supercomputing consortium. We find that at early times the barycentre of the material that ends up in a rich cluster is generally very close to a peak of the initial density field. Furthermore, the mean peculiar velocity of this material agrees well with the linear value at the peak. The late-time growth of peculiar velocities is, however, systematically underestimated by linear theory. At the time when clusters are identified, we find their rms peculiar velocity to be about 40 per cent larger than predicted. Non-linear effects are particularly important in superclusters. These systematics must be borne in mind when using cluster peculiar velocities to estimate the parameter combination $\sigma_8\Omega^{0.6}$.

Key words: galaxies: clusters: general – cosmology: theory – dark matter – large-scale structure of Universe.

1 INTRODUCTION

The motions of galaxy clusters are thought to result from gravitational forces acting over the very large scales on which superclusters are assembled. The rms deviations from uniformity on such scales appear to be small, and so may be adequately described by the linear theory of fluctuation growth. For a linear density field of given power spectrum the rms peculiar velocity is proportional to $\sigma_8\Omega^{0.6}$, where Ω is the cosmic density parameter and σ_8, the rms mass fluctuation in a sphere of radius $8\,h^{-1}\,\mathrm{Mpc}$, is a conventional measure of the amplitude of fluctuations (e.g. Peebles 1993). (As usual, the Hubble constant is expressed as $H_0 = 100\,h\,\mathrm{km\,s^{-1}\,Mpc^{-1}}$.) Distance indicators such as the Tully–Fisher or D_n–σ relations allow the peculiar velocities of clusters to be measured, thus providing a direct estimate of this parameter combination (see, for example, Strauss & Willick 1995).

Essentially the same parameter combination can also be estimated from the *abundance* of galaxy clusters (e.g. White, Efstathiou & Frenk 1993), and a comparison of the two estimates could in principle provide a check on the shape of the assumed power spectrum and on the assumption that the initial density field had Gaussian statistics. In practice this is difficult because of the uncertainties in relating observed cluster samples to the objects for which quantities are calculated in linear theory or measured from *N*-body simulations. The standard linear model was introduced by Bardeen et al. (1986, hereafter BBKS). It assumes that clusters can be identified with 'sufficiently' high peaks of the linear density field after convolution with a 'suitable' smoothing kernel. The peculiar velocity of a cluster is identified with the linear peculiar velocity of the corresponding peak extrapolated to the present day. In the present paper we study the limitations both of this model and of direct *N*-body simulations by comparing their predictions for clusters on a case-by-case basis.

In the next section we summarize both the linear predictions for the growth of peculiar velocities and the BBKS formulae for the values expected at peaks of the smoothed density field. Section 3 then presents our set of *N*-body simulations and outlines our procedures for identifying peaks in the initial conditions and clusters at $z = 0$. Section 4 begins by studying how well the initial barycentres of clusters correspond to peaks; we then show that the

★ E-mail: swhite@mpa-garching.mpg.de
†Present address: Enterprise Architecture Group, Global Securities Industry Group, 1185 Avenue of the Americas, New York, NY 10036, USA.

mean linear velocity of a cluster agrees with the smoothed linear velocity at its associated peak; finally we show that the growth of cluster peculiar velocities is systematically stronger at late times than linear theory predicts. A final section presents a brief discussion of these results.

2 LINEAR PREDICTIONS FOR THE PECULIAR VELOCITIES OF PEAKS

2.1 The growth of peculiar velocities

According to the linear theory of gravitational instability in a dust universe (Peebles 1993), the peculiar velocity of every mass element grows with cosmic factor a as

$$v \propto a\dot{D}, \tag{1}$$

where $a(t)$ is obtained from the Friedman equation

$$\left(\frac{\dot{a}}{a}\right)^2 = \Omega_0 a^{-3} + (1 - \Omega_0 - \Lambda_0)a^{-2} + \Lambda_0, \tag{2}$$

and $D(t)$ is the growth factor for linear density perturbations, $\delta(\boldsymbol{x}, t) = D(t)\delta_0(\boldsymbol{x})$. Ω_0 and Λ_0 are the density parameter and the cosmological constant at $z = 0$, respectively, and we define $a = 1$ at this time. A number of accurate approximate forms are known for the relations between D and a, and can be used to cast the scaling of equation (1) into a more convenient form. We write

$$\dot{D} \equiv \frac{\mathrm{d}D}{\mathrm{d}t} = \frac{\mathrm{d}D}{\mathrm{d}a}\frac{\mathrm{d}a}{\mathrm{d}t}, \tag{3}$$

and substitute for $\mathrm{d}a/\mathrm{d}t$ from the Friedman equation (2). Lahav et al. (1991) give an approximation for $\mathrm{d}D/\mathrm{d}a$ in the combination

$$f(a) \equiv \frac{\mathrm{d}D}{\mathrm{d}a}\frac{a}{D} \approx \left[\frac{\Omega_0 a^{-3}}{\Omega_0 a^{-3} + (1 - \Omega_0 - \Lambda_0)a^{-2} + \Lambda_0}\right]^{0.6}. \tag{4}$$

For $a = 1$ this gives the standard factor $f \approx \Omega_0^{0.6}$ which appears when predicting the peculiar velocities produced by a given overdensity field. Carroll, Press & Turner (1992) used this result to derive an approximation for $D(a)$ itself,

$$D \approx a\, g(a), \tag{5}$$

where

$$g(a) = \frac{5}{2}\frac{\Omega(a)}{\Omega^{4/7}(a) - \Lambda(a) + \left[1 + \frac{\Omega(a)}{2}\right]\left[1 + \frac{\Lambda(a)}{70}\right]}, \tag{6}$$

with

$$\Omega(a) = \frac{\Omega_0}{a + \Omega_0(1 - a) + \Lambda_0(a^3 - a)}, \tag{7}$$

$$\Lambda(a) = \frac{\Lambda_0 a^3}{a + \Omega_0(1 - a) + \Lambda_0(a^3 - a)}. \tag{8}$$

Combining these equations, we obtain an explicit approximation for the growth of peculiar velocities:

$$v \propto f(a)g(a)a^2\sqrt{\Omega_0 a^{-3} + (1 - \Omega_0 - \Lambda_0)a^{-2} + \Lambda_0}. \tag{9}$$

For the simple Einstein–de Sitter case where $\Omega_0 = 1$ and $\Lambda = 0$, these formulae reduce to the exact results $D = a \propto t^{2/3}$ and $v \propto \sqrt{a}$.

Recently, Eisenstein (1997) has shown that the exact solutions for D and $f(a)$ can be given explicitly in terms of elliptic integrals. He also shows that the above approximations always have fractional errors smaller than 2 per cent if $\Omega > 0.1$. We therefore work with the simpler approximate formulae in the present paper.

2.2 The velocities of peaks

The idea that the statistical properties of non-linear objects like galaxy clusters can be inferred from the initial linear density field was developed in considerable detail in the monumental paper of BBKS. If the initial fluctuations are assumed to be a Gaussian random field, they are specified completely by their power spectrum, $P(k)$. Similarly, any smoothed version of this initial field is specified completely by its own power spectrum, $P(k)W^2(kR)$, where $W(kR)$ is the Fourier transform of the spherical smoothing kernel and R is a measure of its characteristic radius. In particular, BBKS showed how the abundance and rms peculiar velocity of peaks of given height can be expressed in terms of integrals over $P(k)W^2(kR)$. The difficulty in connecting this model with real clusters lies in the ambiguity in deciding what smoothing kernel, characteristic scale and peak height are appropriate. Typically the smoothing kernel is taken to be a Gaussian or a top-hat, R is chosen so that the kernel contains a mass similar to the minimum mass of the cluster sample, and the height is assumed sufficient for a spherical perturbation to collapse by $z = 0$.

The smoothed initial peculiar velocity field is isotropic and Gaussian with a three-dimensional dispersion given by

$$\sigma_v(R) \equiv H\Omega^{0.6}\sigma_{-1}(R), \tag{10}$$

where, in the notation of BBKS, σ_j is defined for any integer j by

$$\sigma_j^2(R) = \frac{1}{2\pi^2}\int P(k)W^2(kR)k^{2j+2}\,\mathrm{d}k. \tag{11}$$

The rms peculiar velocity at peaks of the smoothed density field differs systematically from σ_v; BBKS showed that it is given by

$$\sigma_\mathrm{p}(R) = \sigma_v(R)\sqrt{1 - \sigma_0^4/\sigma_1^2\sigma_{-1}^2}. \tag{12}$$

Note that this expression does not depend on the height of the peaks. As shown by BBKS, the velocities of peaks are *statistically* independent of their height.

Throughout this paper we will approximate the power spectra of cold dark matter (CDM) models by the parametric expression of Bond & Efstathiou (1984),

$$P(k, \Gamma) = \frac{Ak}{\{1 + [ak/\Gamma + (bk/\Gamma)^{3/2} + (ck/\Gamma)^2]^\nu\}^{2/\nu}}, \tag{13}$$

where $a = 6.4\,h^{-1}\,\mathrm{Mpc}$, $b = 3.0\,h^{-1}\,\mathrm{Mpc}$, $c = 1.7\,h^{-1}\,\mathrm{Mpc}$, $\nu = 1.13$, and the shape parameter Γ is given for the models discussed below by

$$\Gamma = \begin{cases} \Omega_0 h/[0.861 + 3.8(m_{10}^2\tau_\mathrm{d})^{2/3}]^{1/2} & \text{for } \tau\text{CDM}, \\ \Omega_0 h & \text{otherwise.} \end{cases} \tag{14}$$

In the τCDM case, m_{10} is the τ-neutrino mass in units of 10 keV and τ_d is its lifetime in years (White, Gelmini & Silk 1995). A detailed investigation of this model can be found in the paper by Bharadwaj & Sethi (1998). For the cosmologies used here, we take the values shown in Table 1. Detailed calculations of the power spectrum are actually better fitted by slightly smaller values of Γ than we assume (Sugiyama 1995).

The normalization constant in equation (13) can be related to

the conventional normalization σ_8 by nothing that $\sigma_8 \equiv \sigma_0(8\,h^{-1}\,\mathrm{Mpc})$ and using equation (11) with a top-hat window function, $W_{\rm TH}(x) = 3(x\sin x - \cos x)/x^3$. This corresponds to the linear fluctuation amplitude extrapolated to $z = 0$, and can be matched to observation by fitting either to the cosmic microwave background fluctuations measured by *COBE* or to the observed abundance of rich galaxy clusters. The models of this paper are normalized using the second method (cf. Eke, Cole & Frenk 1996), as reflected by the σ_8 values given in Table 1 together with the other parameters defining the models.

In the following, linear density fields are smoothed either with a top-hat or with a Gaussian. In the latter case the window function is $W_{\rm G}(x) = \exp(-x^2/2)$. It is unclear for either filter how R should be chosen in order to optimize the correspondence between peaks and clusters. We follow previous practice in assuming that cluster samples contain all objects with mass exceeding some threshold $M_{\rm min}$, and then choosing R so that the filter contains $M_{\rm min}$. Hence $M_{\rm min} = 4\pi\bar{\rho}R^3/3$ in the top-hat case and $M_{\rm min} = (2\pi)^{3/2}\bar{\rho}R^3$ in the Gaussian case. The simulations analysed here have $\Omega_0 = 0.3$ or 1.0, and we will isolate cluster samples limited at $M_{\rm min} = 3.5\times10^{14}\,h^{-1}\,\mathrm{M}_\odot$, the value appropriate for Abell clusters of richness one and greater (e.g. White et al. 1993). A detailed discussion of filtering schemes can be found in Monaco (1998) and references therein.

Table 2 gives characteristic filter radii R and values of σ_v and $\sigma_{\rm p}$ from equations (11) and (13) for both smoothings and for all the cosmological models that we consider in this paper; the velocity dispersions quoted are extrapolations to $z = 0$ according to linear theory. The difference between σ_v and $\sigma_{\rm p}$ has often been ignored in the literature when predicting the peculiar velocities of galaxy clusters (e.g. Croft & Efstathiou 1994; Bahcall & Oh 1996; Borgani et al. 1997); for our models the two differ by about 15 per cent. Notice also that, with our choice of filter radii, Gaussian smoothing predicts rms peculiar velocities about 10 per cent smaller than does top-hat smoothing.

Table 1. The Virgo models.

Model	Ω	Λ	h	σ_8	Γ	$z_{\rm Start}$
OCDM	0.3	0.0	0.7	0.85	0.21	119
ΛCDM	0.3	0.7	0.7	0.90	0.21	30
SCDM	1.0	0.0	0.5	0.51	0.50	35
τCDM	1.0	0.0	0.5	0.51	0.21	35

3 THE SIMULATIONS

3.1 The code

The Virgo Consortium was formed in order to study the evolution of structure and the formation of galaxies using the latest generation of parallel supercomputers (Jenkins et al. 1996). The code used for the simulations of this paper is called HYDRA. The original serial code was developed by Couchman, Thomas & Pearce (1995), and was parallelized for CRAY T3Ds as described in Pearce & Couchman (1997). T3D–HYDRA is a parallel adaptive particle–particle/particle–mesh ($\mathrm{AP^3M}$) code implemented in CRAFT, a directive-based parallel FORTRAN developed by CRAY. It supplements the standard $\mathrm{P^3M}$ algorithm (Efstathiou et al. 1985) by recursively placing higher resolution meshes, 'refinements', over heavily clustered regions. Refinements containing more than $\sim10^5$ particles are executed in parallel by all processors; smaller refinements are completed using a task farm approach. This T3D version currently includes a smoothed particle hydrodynamics (SPH) treatment of gas dynamics, but this was not used for the simulations of this paper.

A second version of HYDRA, based on the shared memory and message passing architecture of CRAY, has been written by MacFarland et al. (1998). This can run on CRAY T3Es but does not currently include refinement placing.

The simulations used here were run on the Cray T3D and T3E supercomputers at the computer centre of the Max-Planck-Gesellschaft in Garching, and at the Edinburgh Parallel Computing Centre.

3.2 The simulation set

A set of four matched N-body simulations of CDM universes was completed in early 1997. Each follows the evolution of structure within a cubic region $240\,h^{-1}\,\mathrm{Mpc}$ on a side using 256^3 equal-mass particles and a gravitational softening of $30\,h^{-1}\,\mathrm{kpc}$. The choices of cosmological parameters correspond to standard CDM (SCDM), to an Einstein–de Sitter model with an additional relativistic component (τCDM), to an open CDM model (OCDM), and to a flat low-density model with a cosmological constant (ΛCDM). A list of the parameters defining these models is given in Table 1.

In all models the initial fluctuation amplitude, and so the value of σ_8, was set by requiring that the models should reproduce the observed abundance of rich clusters. Further details of this

Table 2. For each of the models, the following quantities are given: the radius R (second and fifth columns) of the filter used in equation (12); the three-dimensional velocity dispersions σ_v and $\sigma_{\rm p}$ (third, fourth, sixth and seventh columns) obtained using equations (11) and (13) with the given filter radii; the three-dimensional velocity dispersions σ_v and $\sigma_{\rm p}$ (eighth, ninth, eleventh and twelfth columns) obtained using equations (11) and (13) with the given filter radii and the power spectra of the simulations themselves; the rms linear overdensity Δ (tenth and thirteenth columns) smoothed with the given filter radii and extrapolated to $z = 0$; the number of clusters $N_{\rm Cl}$ (fourteenth column) found in the simulations at $z = 0$; the three-dimensional velocity dispersions of peaks (fifteenth and sixteenth columns) in the initial conditions of the simulations using the given filters; the three-dimensional linear velocity dispersions of clusters extrapolated to $z = 0$ (seventeenth column); and the three-dimensional measured velocity dispersion of clusters at $z = 0$ (eighteenth column). The radii are given in $h^{-1}\,\mathrm{Mpc}$, the velocity dispersions in $\mathrm{km\,s^{-1}}$. Top-hat and Gaussian filters are abbreviated as TH and G, respectively.

	Top-hat			Gaussian			Sim TH			Sim Gauss				TH	G	Sim	Sim
(1)	(2)	(3)	(4)	(5)	(6)	(7)	(8)	(9)	(10)	(11)	(12)	(13)	(14)	(15)	(16)	(17)	(18)
Model	R	σ_v	$\sigma_{\rm p}$	R	σ_v	$\sigma_{\rm p}$	σ_v	$\sigma_{\rm p}$	Δ	σ_v	$\sigma_{\rm p}$	Δ	$N_{\rm Cl}$	$\sigma_{\rm Peak}$	$\sigma_{\rm Peak}$	$\sigma_{\rm lin}$	$\sigma_z = 0$
OCDM	10.3	390	349	6.6	366	315	351	300	0.94	321	258	0.96	62	253	266	280	407
ΛCDM	10.3	413	370	6.6	387	334	371	318	0.98	340	272	1.03	69	296	323	300	439
SCDM	6.9	381	334	4.4	349	290	375	325	0.58	342	278	0.60	92	308	318	307	425
τCDM	6.9	509	464	4.4	485	430	464	412	0.57	437	371	0.58	70	392	399	398	535

choice and of other aspects of the simulations can be found in Jenkins et al. (1998). Note that each Fourier component of the initial fluctuation field had the same *phase* in each of these four simulations. As a result there is an almost perfect correspondence between the clusters in the four models.

Because of their finite volume, these simulations contain no power at wavelengths longer than $240\,h^{-1}$ Mpc. Furthermore, Fourier space is sampled quite coarsely on the largest scales for which they do contain power, and so realization-to-realization fluctuations on these scales can be significant. The size of the effects can be judged from Table 2, where we list the values of σ_v and σ_p obtained for each model when the theoretical power spectrum is replaced in equations (11) and (13) by the initial power spectrum of the model itself. These are systematically smaller than the values found before. The difference is primarily a reflection of the loss of large-scale power. In addition, we also ran a second realization of the τCDM model to check on realization-to-realization variations – see below.

3.3 The selection of peaks

We identify peaks in the initial conditions of the simulations by binning up the initial particle distribution on a 128^3 mesh using a cloud-in-cell (CIC) assignment and then smoothing with a Gaussian or a top-hat with characteristic scale R corresponding to $M_{\rm min} = 3.5 \times 10^{14}\,h^{-1}\,{\rm M}_\odot$. A peak is then taken to be any grid-point at which the smoothed density is greater than that of its 26 nearest neighbours. The dimensionless height of a peak, ν, is defined by dividing its overdensity by the rms overdensity, Δ, which we list in Table 2. Again, within the matched set there is a close correspondence between the peaks found in the four models. In addition, the peaks found with Gaussian smoothing correspond closely to those found with top-hat smoothing. In the following we consider only peaks with $\nu > 1.5$.

Particle peculiar velocities are binned up and smoothed in an identical way, and the peculiar velocity of a peak is taken to be the value at the corresponding grid-point. In Table 2 we list the rms peculiar velocity of the peaks found in each model. Again this is scaled up to the value expected at $z = 0$ according to linear theory. It differs slightly from the value predicted by inserting the power spectrum of the simulation directly into equation (13), because there are realization-to-realization fluctuations depending on the *phases* of the Fourier components. As it should, the rms peculiar velocity averaged over all grid-points agrees very well with the value found by putting the simulation power spectrum into equation (11).

3.4 The selection of clusters

We define clusters in our simulations in the same way as did White et al. (1993). High-density regions at $z = 0$ are located using a friends-of-friends group finder with a small linking length ($b = 0.05$), and their barycentres are considered as candidate cluster centres. Any candidate centre for which the mass within $1.5\,h^{-1}$ Mpc exceeds $M_{\rm min}$ is identified as a candidate cluster. The final cluster list is obtained by deleting the lower mass candidate in all pairs separated by less than $1.5\,h^{-1}$ Mpc. In the following we will normally consider only clusters more massive than $M_{\rm min} = 3.5 \times 10^{14}\,h^{-1}\,{\rm M}_\odot$. The number of clusters found in each simulation is listed in Table 2. As already noted, the individual clusters in the different simulations of the matched set correspond closely. Despite the normalization to cluster abundance, it appears as though the SCDM model has significantly more clusters than the others. This is a reflection of its steeper power spectrum together with the value of $M_{\rm min}$ that we have chosen. For $M_{\rm min} = 5.5 \times 10^{14}\,h^{-1}\,{\rm M}_\odot$ all the models have about 20 clusters. The number densities of the clusters in our simulations correspond to the *observed* number density of rich clusters in the Universe.

We define the peculiar velocity of each cluster at $z = 0$ to be the mean peculiar velocity of all the particles within the $1.5\,h^{-1}$ Mpc sphere. The peculiar velocity of the cluster at earlier times is taken to be the mean peculiar velocity of these particles. Consistently with this, we define the position of the cluster at each time to be the barycentre of this set of particles. At $z = 0$ this is very close to, but not identical with, the cluster centre as defined above. We give the rms values of the initial (linear) and final ($z = 0$) peculiar velocities of the clusters in each of our models in Table 2. The initial values have been scaled up to the linear values predicted at $z = 0$. It is clear that these substantially underestimate the actual values, a result that we discuss in more detail below. We note that the present-day properties of clusters in these simulations are considered in much more detail by Thomas et al. (1998).

4 COMPARISON OF THE PEAK MODEL WITH SIMULATIONS

4.1 The cluster–peak connection

The extent to which dark haloes can be associated with peaks of the smoothed initial density field is somewhat controversial. Frenk et al. (1988) concluded that, for appropriate choices of filter scale and peak height, the correspondence is good, whereas Katz, Quinn & Gelb (1993) claimed that 'there are many groups of high mass that are not associated with any peak'. The result of correlating the peaks in the initial conditions of our simulations with the initial positions of our clusters is illustrated in Fig. 1. We consider a peak and a cluster to be associated if their separation is less than $4\,h^{-1}$ Mpc (comoving). We find that for low Ω the barycentres of 70 per cent of the clusters with masses exceeding $3.5 \times 10^{14}\,h^{-1}\,{\rm M}_\odot$ are associated with a peak with $\nu > 1.5$; for high Ω the corresponding fraction is 80 per cent. Most of the remaining clusters are associated with a peak either of slightly lower height or at slightly greater separation. Thus the correspondence of clusters to peaks is relatively good. On the other hand, most peaks with $\nu > 1.5$, and in particular most of the lower ones, are not associated with a cluster. We need ν values exceeding 2 to 2.5 before most peaks have an associated cluster above our mass threshold.

Fig. 1 shows that there is, as expected, a correlation between the height of a peak and the mass of the corresponding cluster. In addition, combining the peak heights with the Δ values from Table 2, we see that the extrapolated *linear* overdensities of the peaks at redshift zero are similar but somewhat larger than the threshold value of 1.69 used in the standard Press–Schechter approach to analysing structure formation.

4.2 Linear peculiar velocities of peaks and clusters

Given that the initial positions of most clusters are near peaks of the smoothed linear density field, it is natural to identify the initial peculiar velocity of a cluster with that at the associated peak. We compare the two for our set of cluster–peak associations in Fig. 2,

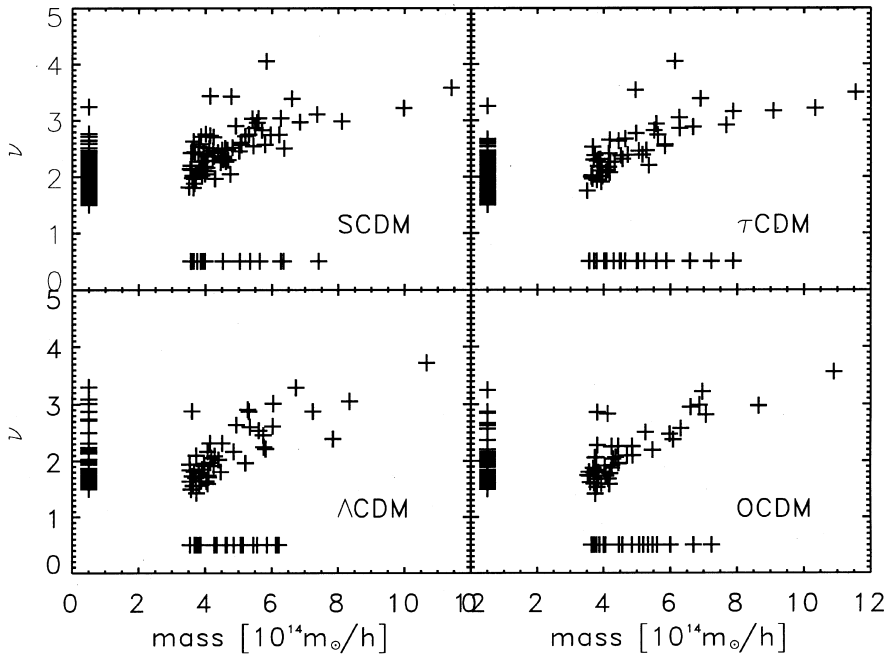

Figure 1. The mass of the clusters in our simulations against the height of the corresponding peaks in the initial conditions, once these are smoothed with a top-hat with the characteristic radius listed in Table 2. All clusters with mass greater than $3.5 \times 10^{14}\, h^{-1}\, \mathrm{M}_{\odot}$ and all peaks with height greater than $\nu = 1.5$ are shown. There are 351, 239, 84 and 83 unmatched peaks in the SCDM, τCDM, ΛCDM and OCDM models, respectively.

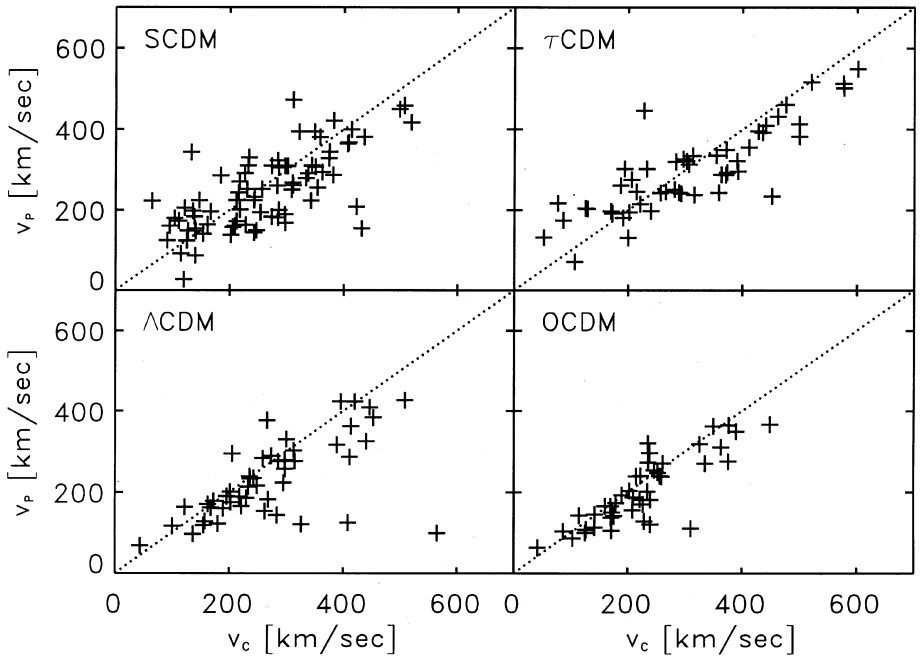

Figure 2. The initial peculiar velocities of clusters in each of our four cosmogonies are compared with the linear peculiar velocities of their associated peaks. The linear peculiar velocity field was smoothed with a top-hat in the same way as the density field in order to obtain the peak peculiar velocities.

again based on top-hat smoothing of the density and peculiar velocity fields using the characteristic radii listed in Table 2. All velocities are scaled up to the expected value at $z = 0$ according to linear theory. The correlation is good for all models, and is similar if Gaussian rather than top-hat smoothing is used. The rms (vector) difference in peculiar velocity between a cluster and its associated peak is 16, 16, 23 and 17 per cent of the corresponding σ_{p} value listed in Table 2 for the OCDM, ΛCDM, SCDM and τCDM simulations respectively. The somewhat larger percentage for the SCDM model is probably a consequence of the greater influence of small-scale power in this case.

We have checked that the distribution of peculiar velocities for peaks is independent both of peak height and of whether a peak is or is not associated with a cluster. The former is a theoretical prediction of BBKS; the latter ensures that the rms velocities predicted for peaks (equations 11 to 13) are applicable to the

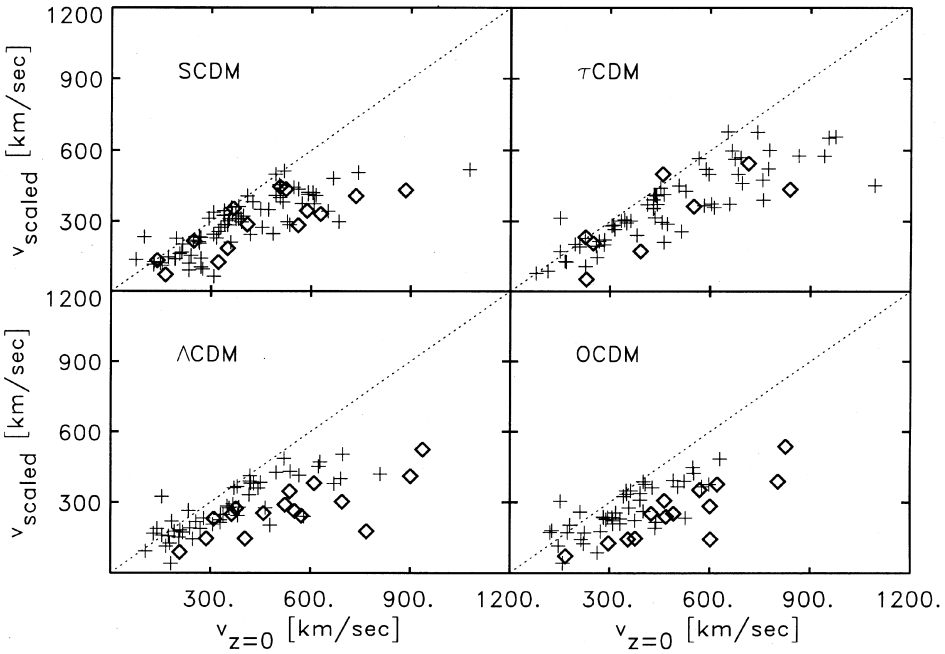

Figure 3. The initial peculiar velocities of clusters in each of our four cosmogonies, scaled up to $z = 0$ using linear theory, are compared with their actual peculiar velocities at $z = 0$. Diamonds denote clusters that have a neighbour within $10\,h^{-1}$ Mpc, while crosses denote more isolated clusters.

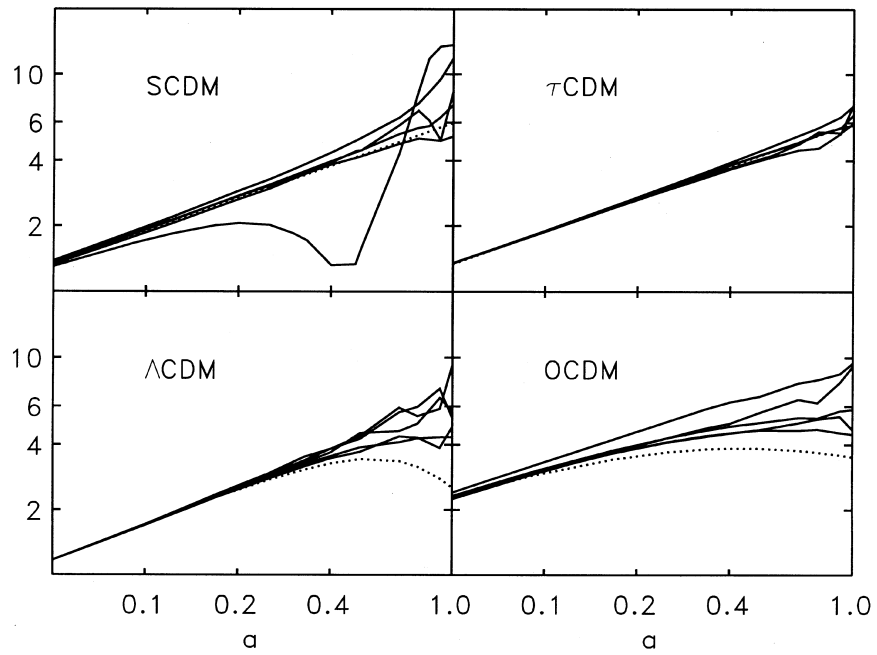

Figure 4. The evolution with expansion factor a of the ratio $|\boldsymbol{v}(a)|/|\boldsymbol{v}_0|$ for five clusters from each of our four cosmogonies (solid lines) is compared with the evolution predicted by linear theory (dotted line). In some of the cases, merging leads to abrupt changes in this ratio – the most impressive case can be seen for one of the SCDM clusters.

subset of peaks identified with clusters. This can be verified explicitly by comparing columns (15), (16) and (17) in Table 2.

4.3 The growth of cluster peculiar velocities

If cluster peculiar velocities grew according to linear theory, the scaled initial velocities discussed in the last section and plotted in Fig. 2 would correspond to the actual velocities of the clusters at $z = 0$. In Fig. 3 we show scatter diagrams in which these two velocities are plotted against each other. It is evident that in fact the agreement is quite poor, and that there is a systematic trend for the true cluster velocity to be larger than the extrapolated linear value. This is reflected in the substantial difference between the rms values of these two quantities listed in Table 2. It is presumably a consequence of non-linear gravitational forces accelerating the clusters.

Some confirmation of this is provided by Fig. 4, where we plot the peculiar velocity in units of its initial value for five clusters

from each of our cosmologies. At early times the peculiar velocities all grow as expected from linear theory (indicated in the figures by a dotted line), but at later times the behaviour is more erratic and most clusters finish with larger velocities than predicted.

It is well known that peculiar velocities decay in low-Ω models (e.g. Peebles 1993). This effect is seen directly in the theoretical curves of Fig. 4, and we have checked that it is indeed present in our simulations by computing the evolution of the mean peculiar velocity for sets of particles that were initially in randomly placed spheres of radius $15\,h^{-1}$ Mpc. A plot similar to Fig. 4 then shows that most sets follow the linear expectation reasonably well, and that their rms follows it extremely closely.

Further evidence that late-time non-linear effects are responsible for the discrepant growth comes from Fig. 3. In this plot, all clusters that have a neighbour within $10\,h^{-1}$ Mpc are indicated with a diamond, while more isolated clusters are indicated by a cross. It is evident that deviations from linear theory are substantially larger for the 'supercluster' objects than for the rest. These objects also have systematically larger peculiar velocities at $z = 0$. Their rms peculiar velocity is around 20 to 30 per cent larger than that of the sample as a whole.

For the τCDM model, we ran a second simulation with different initial phases which we analysed in exactly the same way as our other models. In this case the rms peculiar velocity of the clusters at $z = 0$ is $511\,\mathrm{km\,s^{-1}}$, and their extrapolated rms linear peculiar velocity is $394\,\mathrm{km\,s^{-1}}$. These numbers are very close to the values obtained for the first τCDM realization. Although two simulations are not a good statistical sample, we conclude that the mismatch between the extrapolated linear and the actual peculiar velocities is not an artefact of the particular set of phases in our original simulations.

It might be thought that the anomalous acceleration at late times is a consequence of the relatively smaller radius, $1.5\,h^{-1}$ Mpc, that we use to define our clusters. Material could, perhaps, be ejected asymmetrically from this region during the merging events by which clusters form. We have searched for such effects by redefining clusters to be all the material contained within a radius of 3 or $5\,h^{-1}$ Mpc, and then repeating the analysis for the same set of objects as before. In most cases this turned out to make very little difference to either the initial or the final velocities, and it did nothing to reduce the discrepancy between them. The relevant non-linear effects are acting on significantly larger scales. We repeated this procedure, going out as far as $25\,h^{-1}$ Mpc from the cluster centre. At a radius of $10\,h^{-1}$ Mpc, the difference between the rms peculiar velocity and the extrapolated rms linear peculiar velocity is only 10 per cent. By a radius of $20\,h^{-1}$ Mpc, the numbers have finally converged.

The discrepancy between the rms peculiar velocity of clusters and their extrapolated rms linear peculiar velocity is also not a consequence of our smoothing of the density field. With our choice of smoothing filter, the linear peculiar velocities of the clusters accurately match those of their associated peaks. In addition, their rms matches the value predicted for all peaks by linear theory when the simulated realization of the power spectrum and the proper expression for peak peculiar velocities (equation 13) are used. Previous work (e.g. Borgani et al. 1997) has tried to match *N*-body data with linear theory by tuning the filter scale. Our results undermine the physical basis for such a procedure.

5 CONCLUSIONS

We have investigated the peculiar velocities predicted for galaxy clusters by theories in the cold dark matter family. A widely used hypothesis identifies rich clusters with high peaks of a smoothed version of the linear density fluctuation field. Their peculiar velocities are then obtained by extrapolating the similarly smoothed linear peculiar velocities at the positions of these peaks. We have tested this using a set of four large high-resolution *N*-body simulations. We identify galaxy clusters at $z = 0$ and then trace their particles back to earlier times. In the initial density fields of the low- and high-density models, the barycentres of 70 and 80 per cent, respectively, of clusters with masses exceedings $3.5 \times 10^{14}\,h^{-1}\,\mathrm{M}_\odot$ lie within $4\,h^{-1}$ Mpc (comoving) of a peak with $\nu > 1.5$. Furthermore, the mean linear peculiar velocity of the cluster material agrees well with that of the associated peak.

However, the late-time growth of peculiar velocities is systematically underestimated by linear theory. At the time when clusters are identified, i.e. at $z = 0$, we find that their rms peculiar velocity is about 40 per cent larger than the extrapolated linear value. Non-linear effects are particularly important in superclusters; the rms peculiar velocities of clusters that are members of superclusters are about 20 per cent to 30 per cent larger than those of isolated clusters.

ACKNOWLEDGMENTS

The simulations were carried out on the Cray T3Ds and T3Es at the computer centre of the Max-Planck-Gesellschaft in Garching, and at the Edinburgh Parallel Computing Centre. Post-processing was done on the IBM SP2 at the computer centre of the Max-Planck-Gesellschaft in Garching. We thank George Efstathiou and John Peacock for valuable comments. JMC thanks Matthias Bartelmann, Antonaldo Diaferio, Adi Nusser, Ravi Sheth, Neta Bahcall and Mirt Gramann for numerous helpful and interesting discussions, and Volker Springel for providing his smoothing code. This work was supported in part by the EU's TMR Network for Galaxy Formation. CSF acknowledges a PPARC Senior Research Fellowship.

REFERENCES

Bahcall N. A., Oh S. P., 1996, ApJ, 462, L49
Bardeen J. M., Bond J. R., Kaiser N., Szalay A. S., 1986, ApJ, 304, 15 (BBKS)
Bharadwaj S., Sethi S. K., 1998, ApJS, 114, 37
Bond J. R., Efstathiou G., 1984, ApJ, 285, L45
Borgani S., Da Costa L. N., Freudling W., Giovanelli R., Haynes M. P., Salzer J., Wegner G., 1997, ApJ, 482, L121
Carroll S. M., Press W. H., Turner E. L., 1992, ARA&A, 30, 499
Couchman H. M. P., Thomas P. A., Pearce F. R., 1995, ApJ, 452, 797
Croft R. A. C., Efstathiou G., 1994, MNRAS, 268, L23
Efstathiou G., Davis M., Frenk C. S., White S. D. M., 1985, ApJS, 57, 241
Eisenstein D. J., 1997, astro-ph/9709054
Eke V. R., Cole S., Frenk C. S., 1996, MNRAS, 282, 263
Frenk C. S., White S. D. M., Davis M., Efstathiou G., 1988, ApJ, 327, 507
Jenkins A. et al., 1996, in Persic M., Salucci P., eds, ASP Conf. Ser. Vol. 117, Dark and Visible Matter in Galaxies and Cosmological Implications. Astron. Soc. Pac., San Francisco, p. 348
Jenkins A. et al., 1998, ApJ, 499, 20
Katz N., Quinn T., Gelb J. M., 1993, MNRAS, 265, 689
Lahav O., Lilje P. B., Primack J. R., Rees M. J., 1991, MNRAS, 251, 128
MacFarland T., Couchman H. M. P., Pearce F. R., Pichlmaier J., 1998, New Astron., 3, 687
Monaco P., 1998, Fundam. Cosm. Phys., 19, 157

Pearce F. R., Couchman H. M. P., 1997, New Astron., 2, 411
Peebles P. J. E., 1993, Principles of Physical Cosmology. Princeton Univ. Press, Princeton, NJ
Strauss M. A., Willick J. A., 1995, Phys. Rep., 261, 271
Sugiyama N., 1995, ApJS, 100, 281
Thomas P. A. et al., 1998, MNRAS, 296, 106
White M., Gelmini G., Silk J., 1995, Phys. Rev. D., 51, 2669
White S. D. M., Efstathiou G., Frenk C. S., 1993, MNRAS, 262, 1023